# Quantized charge pumping by surface acoustic waves in ballistic quasi-1D channels

Vyacheslavs Kashcheyevs,[1, *] Amnon Aharony,[1, 2] and Ora Entin-Wohlman[1, 2, 3]

[1]*School of Physics and Astronomy, Raymond and Beverly Sackler faculty of Exact Sciences,*
*Tel Aviv University, Tel Aviv 69978, Israel*
[2]*Department of Physics, Ben Gurion University, Beer Sheva 84105, Israel*
[3]*Albert Einstein Minerva Center for Theoretical Physics*
*at the Weizmann Institute of Science, Rehovot 76100, Israel*
(Dated: February 24, 2004)

Adiabatic pumping of electrons induced by surface acoustic waves (SAWs) in a ballistic quasi-1D quantum channel is considered using an exactly solvable tight-binding model for non-interacting electrons. The single-electron degrees of freedom, responsible for acoustoelectric current quantization, are related to the transmission resonances. We study the influence of experimentally controllable parameters (SAW power, gate voltage, source-drain bias, amplitude and phase of a secondary SAW beam) on the plateau-like structure of the acoustoelectric current. The results are consistent with existing experimental observations.

PACS numbers: 73.23.-b, 73.50.Rb, 73.40.Ei

## I. INTRODUCTION

Single electron transport through low-dimensional mesoscopic structures, driven by surface acoustic waves (SAWs), is a subject of active experimental [1, 2, 3, 4, 5, 6, 7, 8, 9] and theoretical [10, 11, 12, 13, 14, 15, 16, 17, 18] research, with potential applications in metrology [19] and new computation technologies [20]. In a typical experimental setup, a quasi-one dimensional ballistic channel is defined in a AlGaAs/GaAs heterostructure and a SAW is launched in the longitudinal direction at a frequency $\omega/2\pi$ of several GHz. Under appropriate conditions, the acoustoelectric dc current $I$ exhibits a staircase plateau-like structure as function of the gate voltage (which controls the depletion of the channel) and of the SAW power. At the plateaus, the current saturates at quantized values $I = e(\omega/2\pi)m$, corresponding to the transfer of an integer number $m$ of electrons per each period of the SAW (here $e$ is the electron charge). The first plateau is the most flat and robust to changes in the control parameters; the higher plateaus become less and less pronounced as the plateau number $m$ is increased. In addition, the effect of factors such as source-drain bias [1, 2, 5], temperature [1, 7], gate geometry [4], a secondary SAW beam [2, 4], and perpendicular magnetic field [5] on the staircase structure and the quality of the first plateau have been studied experimentally.

In the experiment, the plateaus are observed below the conductance pinch-off, when electrons in the source and in the drain reservoirs are separated by a potential barrier. This observation forms the basis for the simple qualitative explanation of the quantized transport which has been proposed in the first experimental report [1] and further refined in Refs. 4, 10, and 11. They argue that when the wavelength $\lambda$ of the SAW is comparable

with the size of the depleted region $L$ (as it is in the experiments [1, 2, 4]), a single potential well forms on top of the static barrier. This potential well then acts as a dynamic quantum dot, which can hold an integer number of electrons due to the Coulomb blockade effect. The captured electrons are transferred from one side of the barrier to the other, with possible quantization errors due to back-tunnelling [10, 11]. In the above description, the formation of the quantum dot and the transport of the localized electrons are treated separately. Particular effects which have been studied theoretically within this picture are the non-adiabatic effects at the quantum dot's formation stage [12], and the classical dynamics of the already confined interacting electrons [15].

A different perspective on the problem has been suggested in Refs. 16 and 21. This approach relates the acoustoelectric transport to adiabatic quantum pumping of non-interacting electrons. The external potential, generated by the SAWs and by the control gates, is viewed as a perturbation acting on a coherent quantum wire [22]. The resulting "staircase" structure of the acoustoelectric current and its dependence on model parameters within this approach have been studied in Refs. 16 and 18, using the adiabatic approximation in conjunction with an exactly solvable one-dimensional (1D) tight-binding model. This theory yields a crossover from a non-quantized acoustoelectric transport to the quantized limit as the SAW power and/or the static barrier height are increased. Although this picture requires the Coulomb interaction in order to set the energy scale of the problem [11, 12, 15], the main qualitative features of the experiment can be reproduced within a model of non-interacting spinless electrons [13, 16].

In this paper we extend the results of Ref. 16. The mechanism of quantized transport is elucidated by using a resonance approximation for adiabatic pumping [23]. Both current quantization and transmission resonances are determined by the quasi-bound states of the electrons captured by a moving potential well. New effects,

*e-mail: slava@latnet.lv

including the influence of a counter propagating SAW, static potential asymmetry and source-drain bias on the number and shape of the quantization steps, are considered. We compare our qualitative conclusions with the published theoretical and experimental results. In particular, tuning the amplitude and the phase of a weak secondary SAW is found to improve the quantization by accordance with an earlier experimental report [4]. For this effect, we propose a new quantitative relation between the phase and the amplitude of the optimal secondary SAW which can be easily checked using existing experimental setups.

The results are presented as follows. In Section II, we describe the model [16] and the algorithms for calculating the adiabatic current. In Section III, we explain the formation of the integer plateaus and make quantitative analytic estimates by applying the resonance approximation [23] to the model of Ref. 16. Building on these results we analyze in Sec. IV additional factors, not described previously, such as reflected SAWs, source-drain bias and gradual screening of the pumping potential. Finally, a discussion of our results in the context of related work is presented in Sec. V, together with several conclusions.

## II. THE MODEL

### A. The tight-binding Hamiltonian

The model consists of a nanostructure and two 1D leads connecting its ends to the electronic reservoirs (Fig. 1). The leads are modelled by two chains of sites with vanishing on-site energies and nearest-neighbors hopping amplitudes $-J$. An electron moving in the lead has the energy $E(k) = -2J \cos ka$, where $k$ is the wave vector and $a$ is the lattice constant.

The nanostructure represents the SAW-affected part of the quasi-1D channel. It is described by $N$ tight-binding sites $n = 1, 2, \ldots N$, that form a chain of length $L = (N-1)a$. The non-zero elements of its Hamiltonian matrix, $\mathcal{H}_0(t)$, are constant nearest-neighbors hopping amplitudes $-J_d$ and diagonal time-dependent on-site energies $\epsilon_n(t)$. The connection between the ideal leads and the time-dependent part of the constriction is introduced through a hopping amplitude $-J_l$ ($-J_r$) between the left (right) lead and the site 1 ($N$) of the nanostructure. The resulting full Hamiltonian of the quantum wire will be denoted $\mathcal{H}$. In the trivial case where $J_l = J_r = J_d = J$ and $\epsilon_n = 0$, $\mathcal{H}$ describes an ideal 1D tight-binding lattice. The time-dependence of the on-site energies $\epsilon_n(t)$ reflects the SAW-induced piezoelectric potential, which is responsible for the pumping effect. The simplest case is that of a single running wave as introduced in Ref. 16,

$$\epsilon_n(t) = -V_g + P \cos(\omega t - qx_n) . \quad (1)$$

Here, $V_g$ is the gate voltage (in energy units), $q$ is the wave-vector of the SAW, and $P$ is the amplitude of the
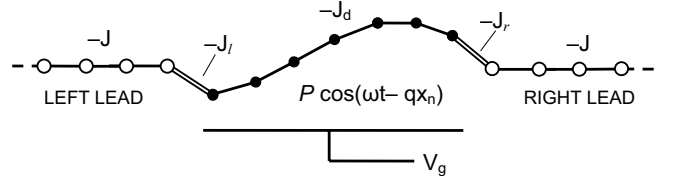


FIG. 1: One-dimensional tight binding model for SAW-induced pumping.

piezoelectric potential, induced by a SAW running from left to right (for $q > 0$). The origin of the spatial coordinate $x_n = (n-1)a - L/2$ is chosen to be at the middle of the channel.

### B. The acoustoelectric current

The adiabatically-pumped current flowing between two reservoirs with equal electrochemical potentials $\mu_l = \mu_r$, is usually calculated using the Brouwer formula [24, 25]. We use an equivalent formalism, developed in Ref. 22, which also includes the effects of a finite bias $eV_{SD} \equiv \mu_l - \mu_r \neq 0$. The total instantaneous current, $I_\alpha(t)$, of spinless electrons from the lead $\alpha = l, r$ into the nanostructure consists of two parts, $I_\alpha(t) = I_\alpha^{\text{pump}} + I_\alpha^{\text{bias}}$. These two parts can be conveniently written down using the instantaneous scattering states $|\Psi_\alpha(t)\rangle$ (normalized to a unit flux), the instantaneous transmission coefficient $\mathcal{T}(t)$ and the overall scattering phase $\theta(t)$ of the nanostructure, [22]

$$I_\alpha^{\text{pump}} = \frac{e}{4\pi\hbar} \int dE \, \langle \Psi_\alpha(t)| \dot{\mathcal{H}} |\Psi_\alpha(t)\rangle \, \frac{\partial(f_l + f_r)}{\partial E}, \quad (2)$$

$$I_\alpha^{\text{bias}} = \frac{e}{2\pi\hbar} \int dE \left\{ (f_l - f_r) \mathcal{T} + \frac{\hbar}{2} \frac{\partial(f_l - f_r)}{\partial E} \mathcal{T} \dot{\theta} \right\}. \quad (3)$$

Here $f_\alpha(E) = 1/[1 + e^{\beta(E-\mu_\alpha)}]$ is the Fermi distribution with $\beta = 1/k_B T$ ($T$ is the temperature). If the system is unbiased, then $I_\alpha^{\text{bias}} = 0$ and Eq. (2) can be shown to reproduce [22, 23] the Brouwer formula [24, 25]. On the other extreme, if no pumping potential is applied, $I_\alpha^{\text{pump}} = 0$ and Eq. (3) leads to the Landauer formula [26] for the conductance, $G = (e^2/h)\mathcal{T}$.

For most of the discussion we assume both the bias voltage $V_{SD}$ and the temperature $T$ to be zero. In this case only electrons at the Fermi energy $\mu_l = \mu_r = E_F$ participate in the scattering. Solving the scattering problem for the potential (1) and using Eq. (2) yields the charge $Q$ pumped over one period (the average dc com-

ponent of the current) [16],

$$Q = \int_0^{2\pi/\omega} dt\, I_l^{\text{pump}}(t) = \frac{e\tilde{J}_l \sin ka}{\pi} \int_0^{2\pi/\omega} dt \sum_{n=1}^N \dot{\epsilon}_n |g_{n,1}|^2 , \tag{4}$$

$$[g^{-1}]_{n,n'} = [E\boldsymbol{I} - \mathcal{H}_0]_{n,n'} + \delta_{n,n'}\, e^{ika}\left(\delta_{n,1}\tilde{J}_l + \delta_{n,N}\tilde{J}_r\right) , \tag{5}$$

where $\tilde{J}_{l;r} \equiv J_{l;r}^2/J$ and $k$ is the Fermi wavenumber, $E_F \equiv E(k)$. The instantaneous transmission is

$$\mathcal{T}(t) = 4|g_{N,1}|^2\, \tilde{J}_l \tilde{J}_r\, \sin^2 ka . \tag{6}$$

The integrand in Eq. (4) is a meromorphic function of $z = \exp(i\omega t)$, with $2N$ pairs of complex conjugate poles. Therefore, the integration of Eq. (4) may be carried out exactly, once the positions of the poles are determined by solving numerically the corresponding algebraic equation of degree $2N$.

### C. Resonance approximation

The second term on the r.h.s. of Eq. (5) is the self-energy addition to the Green's function of the isolated channel, due to the coupling to the external leads. When the latter is sufficiently small, the total pumped charge can be divided into contributions from separate single-particle levels of $\mathcal{H}_0$. A systematic development of this approach leads to the resonance approximation for pumping, which is discussed in detail in Ref. 23. Here we summarize the resulting algorithm for calculating the pumped charge in the this approximation.

1. Solve the instantaneous eigenvalue problem $\sum_{n'} [\mathcal{H}_0]_{n,n'} \psi_{n'}^{(m)} = E_m \psi_n^{(m)}$ and obtain the approximate resonance energies $E_m(t)$.

2. Calculate the time-dependent decay widths of each resonance into each lead,

$$\left\{\Gamma_l^{(m)}, \Gamma_r^{(m)}\right\} = \left\{\tilde{J}_l|\psi_1^{(m)}|^2, \tilde{J}_r|\psi_N^{(m)}|^2\right\} \sin ka . \tag{7}$$

3. For each $m$, find all such times $t_{m,j}$ at which the resonance condition $E_m(t_{m,j}) = E_F$ is satisfied.

4. At each resonance time $t = t_{m,j}$, compute the partial charge transferred between the left lead and the $m$th quasibound state in the channel,

$$\Delta Q_{m,j} = \left. \frac{e\,\Gamma_l^{(m)}}{\Gamma_l^{(m)} + \Gamma_r^{(m)}} \right|_{t=t_{m,j}} . \tag{8}$$

5. Calculate the total charge pumped from left to right[1]:

$$Q^{\text{res}} = -\sum_{m,j} \Delta Q_{m,j}\, \text{sgn}\,\dot{E}_m(t_{m,j}) , \tag{9}$$

or set $Q^{\text{res}} = 0$ if no resonances were found in step 3.

The algorithm has a direct physical interpretation [23]. Whenever the energy $E_m$ of a (quasi-)bound state crosses the Fermi level $E_F$, an electron either occupies ("loading") or leaves ("unloading") this state. The corresponding unit pulse of current is distributed between the channels proportionally to the $\Gamma_\alpha^{(m)}$'s. Except for specifically designed Hamiltonians $\mathcal{H}_0(t)$, $Q^{\text{res}} \to Q$ in the limit of vanishing couplings $\Gamma_\alpha^{(m)} \to 0$.

The resonance approximation fails when either (i) the total width of a particular resonance is larger than the distance to the next energy level; or (ii) the partial decay widths $\Gamma_{l;r}^{(m)}$ change considerably while the system is at resonance [23]. As discussed in detail in the following section, these restrictions become significant for the non-quantized transport, but have little influence on the shape of the current quantization steps. In all the cases in which the resonance approximation is inadequate, we rely on the results of an exact calculation.

## III. FORMATION OF QUANTIZATION STEPS

### A. Application of the resonance approximation

The results of a full calculation (as outlined in Sec. II B) show [16] that the pumped charge, $Q$, follows a staircase-type dependence on the gate voltage, $V_g$, and/or on the SAW amplitude, $P$, for a wide range of the model parameters. This 'quantization' can be related to the structure of the transmission resonances [23, 27, 28]. We first establish this relation quantitatively and then use it to analyze various aspects of the model.

The calculation of the pumping curve can be visualized using a diagram like the one shown in Fig. 2. First, one plots the instantaneous eigenvalues $E_m$ for $V_g = 0$ as function of time $\omega t$ (curves in the right panel of Fig. 2). The small circles on the top of each curve show the time evolution of the corresponding partial charge $\Delta Q$: the diameter of each circle is proportional to $|\Delta Q/e| < 1$; shading is determined by the sign — black (•) for $\dot{E}_m < 0$ ("loading") and white (○) for $\dot{E}_m > 0$ ("unloading"). Once the eigenvalue diagram is constructed, the set of resonances for each particular value $V_g$ of the gate

---

[1] Due to charge conservation, it is sufficient to calculate the charge transfer from the left reservoir. Therefore, the channel index $\alpha$ is fixed to $\alpha = l$ in Eqs. (8) and (9).
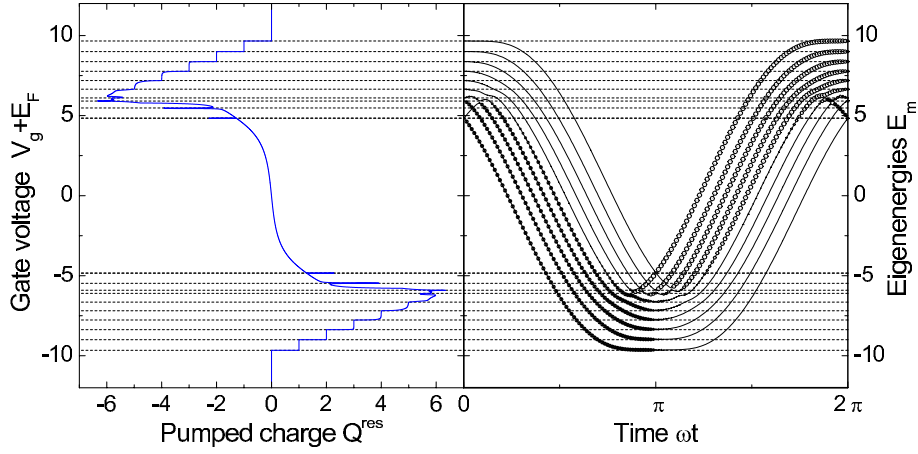
FIG. 2: (Color online) Construction of the pumping curve $Q^{\mathrm{res}}(V_g)$ in the resonance approximation. Right panel: instantaneous energy levels of $\mathcal{H}_0$ at $V_g = 0$ as function of time. Left panel: pumped charge $Q^{\mathrm{res}}$ (in units of $e$) as function of gate voltage. Horizontal dashed lines show the correspondence between sharp features in the pumping curve (left), and the change in the number of energy levels at resonance (right); see text for a detailed discussion. All energies are given in units of $J_d$; the parameters of the potential are: $P = 8J_d$, $\lambda = 4L$, $N = 10$.

voltage is determined graphically: a horizontal line with ordinate $E_F + V_g$ crosses the eigenvalue curves in the right panel at the points where the resonance equation $V_g + E_m(V_g = 0) = E_F$ is satisfied (step 3 of the algorithm). The abscissas of the crossing points determine the resonance times $t_{m,j}$ to be used in Eqs. (8) and (9). (The dashed horizontal lines in Fig. 2 mark the extrema of the eigenvalue curves, and thus correspond to particular values of $V_g$ at which the number of resonances changes.) Finally, the total pumped charge, $Q^{\mathrm{res}}(V_g)$, is calculated by summing up the contributions to Eq. (9): the magnitude and the sign of each term is given by the small circle at the respective crossing point in the right panel. The resulting pumping curve $Q^{\mathrm{res}}(V_g)$ is plotted in the left panel of Fig. 2.

Several aspects of the model are illustrated by the construction in Fig. 2. One can see that the quantization of the pumped charge is caused by electronic (hole) states with the lowest (highest) energy. When resonances occur, (namely, at $\{t_{m,j}\}$), these states are *localized* near one of the channel exits — either $\Gamma_l/\Gamma_r \ll 1$ or $\Gamma_l/\Gamma_r \gg 1$ — and therefore transfer almost integer charges [Eq. (8)]. The number of steps counts the number of localized states involved.

The exact integration [Eq. (4)] takes into account the "external" parameters of the model, $ka$, $\tilde{J}_l$ and $\tilde{J}_r$, which are ignored in the resonance approximation. In the following, we will consider only symmetric couplings, $\tilde{J}_l = \tilde{J}_r \equiv \tilde{J}$. We have calculated the exact pumped charge, $Q(V_g)$, for several values of the "external" parameters, but with the same pumping potential as in Fig. 2. Representative results are shown in Fig. 3 along with the approximate $Q^{\mathrm{res}}(V_g)$ from Fig. 2 [thin (blue) line]. For sufficiently small $\tilde{J}$, the exactly calculated curves contain integer steps and sharp, non-quantized features at large values of $V_g$ (e.g., the spikes marked by small arrows in

Fig. 3). The first steps are robust and do not change their positions as $\tilde{J}$ and $ka$ are varied (except for a trivial shift of $E_F$). The top of the pumping curve and the spikes are more vulnerable: as $\tilde{J}$ is increased, the upper steps and the sharp features shift and become rounded. Narrow spikes disappear for $\tilde{J} = J_d$ and $ka$ close to the center of the band [see curve (c) in the right panel of Fig. 3].

The resonance approximation reproduces all the details of the exact calculation for $\tilde{J} \ll J_d$, because the resonance widths in Eq. (7) vanish in the limit of $\tilde{J} \to 0$. The non-generic sharp features are determined by the surroundings of level anti-crossings (see Fig. 2), where the corresponding level spacings are tiny. As we expect form the validity condition (i) in Sec. II C, the finite resonance width effects are most important in this region. Indeed, the discrepancies between the exact and the approximate curves in Fig. 3 are well correlated with the fact that the shifts and the widths of the resonance levels for a tight-binding model are proportional to $\tilde{J} \cos ka$ and $\tilde{J} \sin ka$, respectively [Eq. (7)].

We have made a similar comparison between the exact integration and the resonance approximation for several sets of "internal" parameters, $P/J_d$, $\lambda/L$, and $N$. The most important conclusion is that the stair-case structure of the pumping curve can be reliably estimated using the resonance approximation. Hence, we will utilize this useful technique in the following as a source for various analytic estimates that will be further checked versus exact calculations.

## B. SAW parameters and the number of quantization steps

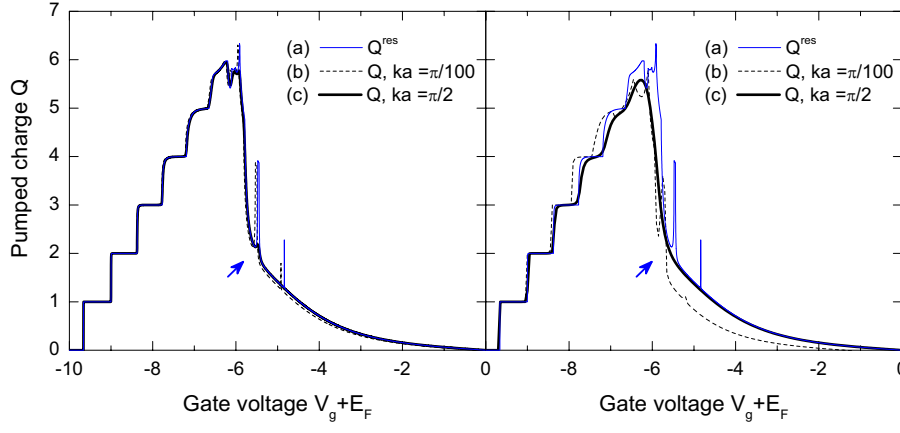For the lowest part of the spectrum (which is relevant for the quantized transport), the on-site energies (1) can

FIG. 3: (Color online) Pumped charge versus gate voltage for different external parameters: $\tilde{J} = 0.16 J_d$ (left panel), $\tilde{J} = 1 J_d$ (right panel), calculated in the resonance approximation (a) and exactly for the bottom of the band (b) and at the band center (c). Parameters of the potential are the same as in Fig. 2.

be treated as a potential function of a continuous spatial coordinate $x_n$. For $\lambda > L$, only one minimum of this potential can be located inside the SAW-affected part of the channel. The position of this minimum $x_0(t) = (t - t_0)v$ moves with the sound velocity $v = \omega/q$ and passes through the middle of the channel at time $t_0 = \omega^{-1}(\pi + 2\pi \times \text{integer})$. Electronic states localized in this moving potential well can be approximated by simple harmonic oscillator wave-functions [16]. The corresponding energy spectrum is $E_m = -P - 2J_d + \Delta(m - 1/2)$, $m = 1, 2, \ldots$, with a constant spacing $\Delta/J_d = qa\sqrt{2P/J_d}$. The lowest energy wave-function is approximately a Gaussian,

$$\psi_n^{(1)}(t) = \left(\xi^2\,\pi/2\right)^{-1/4}\,\exp\{-[x_n - x_0(t)]^2/\xi^2\}, \quad (10)$$

with $\xi \equiv 2a\sqrt{J_d/\Delta}$. The localization length of the higher levels can be estimated as $\xi_m = \xi\sqrt{m}$.

The harmonic approximation is valid as long as the wave-packet is driven adiabatically by a parabolic well and is not perturbed neither by the ends of the channel, nor by the "hills" of the cosine-shaped potential profile. This implies the validity condition

$$\xi_m \ll \min[L/2 - |x_0(t)|, \lambda/2]. \quad (11)$$

In order to illustrate the above reasoning, we draw the attention of the reader to a set of constant and equidistant energy levels $E_m(t)$ in the right panel of Fig. 2, in the vicinity of $\omega t = \pi$. The lowest energy level follows the harmonic approximation as long as the parabolic minimum is located inside the channel, that is for the fraction $\lambda/L = 1/4$ of the full period. Higher energy levels remain constant for shorter times, since their respective localization lengths entering Eq. (11) are longer. The harmonic structure of the energy levels translates into a sequence of equidistant steps in the pumping curve, $Q(V_g)$, with the same energy spacing $\Delta$, as shown in the left panel of Fig. 2. At each value of gate voltage, $V_g^{(m)} = E_m - E_F$, a new pair of resonances and another step in the pumping

curve emerge. The plateaus are rather flat because the resonant states at the loading (unloading) moments are well localized at the entrance (exit) of the channel.

The number of quantization steps, $N_{\text{steps}}$, is limited by two competing mechanisms. The first limit is set by the number, $N_1$, of localized states that can be transferred below the Fermi energy. If $x_n$ can be considered as continuous, the localization condition is roughly the same as the validity condition (11) for the harmonic approximation. For $L < \lambda$ it follows from $\xi_{N_1} = L/2$ that $N_1 = L^2\Delta/(16J_d a^2) = (\pi\sqrt{2}/8)\,N(L/\lambda)\sqrt{P/J_d}$. On the other hand, for large enough $P$ the discreteness of the tight-binding grid cannot be neglected. For a rough estimate, we assume that the continuous approximation breaks down if it yields an average distance $\xi_m/m$ between the successive zeros of the $m$th wave-function, which is smaller than the inter-site spacing $a$. This happens for $m > N_2$, where $N_2 = N^2/(4N_1)$. Putting the two limits together we estimate the number of quantization steps, $N_{\text{steps}}$, as the integer closest to $\min(N_1, N_2)$. By adjusting the parameters one can obtain at best a sequence of $N/2$ steps. The optimal parameters $L = 0.3\lambda$, $N = 6$, $P = 8J_d$ of Ref. 16 indeed yield $N_{\text{steps}} \approx N_1 = 2.83 \approx N_2 \approx N/2$. The decrease in the number of steps with increasing $L/\lambda$ reported in Ref. 16 corresponds to the tight-binding limited regime $N_{\text{steps}} \approx N_2 \propto \lambda/L$.

Despite a certain inherent uncertainty of our estimates, they prove useful for understanding the effect of changing the amplitude and the wavelength of the SAW (Fig. 4). In Fig. 4a, the number of steps is close to optimal, $N/2 = 5$, and is limited by the localization criterion $N_{\text{steps}} \approx N_1 = 3.9$. Increasing $P$ by a factor of 4 (Fig. 4b) reduces the number of steps due to discrete lattice effects: $N_{\text{steps}} \approx N_2 = 3.2$. One can clearly see that for higher energy levels (close to the band center) the tight-binding coupling $J_d$ is no longer relevant: $E_m(t)$ with $m > N_2$ follow a sequence of cosine curves $P\cos(\omega t + \delta\phi)$ with equal
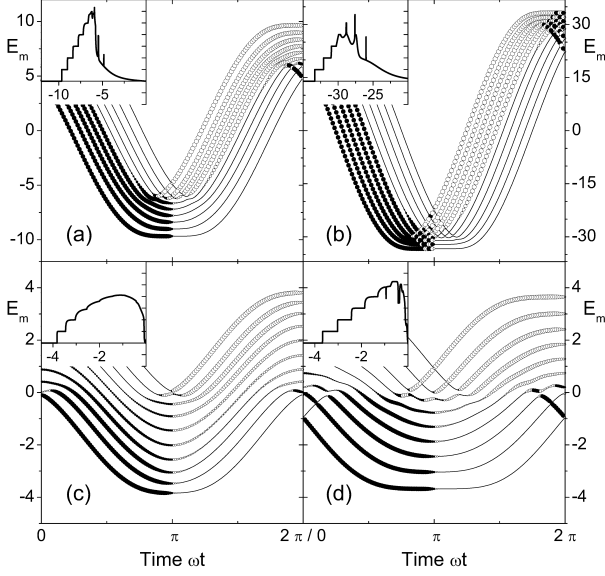
FIG. 4: Instantaneous eigenenergies $E_m$ (in units of $J_d$) for $V_g = 0$, $N = 10$ and (a) $P = 8J_d$, $\lambda = 4L$; (b) $P = 32J_d$, $\lambda = 4L$; (c) $P = 2J_d$, $\lambda = 4L$; and (d) $P = 2J_d$, $\lambda = 2L$. Insets: the pumped charge $Q^{\mathrm{res}}$ as function of the scaled gate voltage $V_g + E_F$; the distance between the ticks on the ordinate axis is equal to a unit charge.

phase differences $qa$. These curves correspond to the individual on-site energies $\epsilon_n(t)$. In this regime the hopping amplitude $J_d$ leads only to tiny anti-crossings between the energy levels, which in turn give rise to the sharp peak-like structure in the pumping curve. The effects of the tight-binding approximation become less pronounced as $P$ is reduced below the optimum (Fig. 4c). In this case $N_{\mathrm{steps}} \approx N_1 = 1.96$ and the peaks in the pumping curve are suppressed. The missing steps can be brought back by shortening the wave-length, as shown in Fig. 4d. The estimated number of steps is now the same as in the original case (a). However, the non-parabolic shape of the potential minimum is more pronounced. Note that in case (d) the flat region for $E_0(t)$ extends over half of the period, since $\lambda = 2L$.

## IV. PERTURBATIONS OF THE PUMPING POTENTIAL

The pumping potential in Eq. (1) is of a rather high symmetry. Small perturbations – such as a static impurity or a reflected SAW — can change the shape and the position of the current quantization steps. In order to explore these effects, we add to $\epsilon_n(t)$ a smooth function of $x_n$ and $t$,

$$\epsilon_n(t) = -V_g + P \cos(\omega t - q x_n) + U(x_n, t). \quad (12)$$

Similarly to the situation discussed above, the structure of the relevant energy levels can be analyzed using the

harmonic approximation, provided that $U(x_n, t)$ changes slowly and the travelling wave-packet is well localized: $\xi_m \, \partial U(x, t)/\partial x \ll \Delta$. The first-order approximation for the instantaneous energy,

$$E_m(t) = -P - 2J_d + \Delta(m - 1/2) + U(x_0(t), t), \quad (13)$$

is valid for $|x_0(t)| \lesssim \frac{L}{2} - \xi_m$ (we consider the case $\lambda > L$). Note that $x_0(t)$ is the position of the potential well minimum, and $x_0(t_0) = 0$ (the middle of the channel). Now even within the harmonic approximation $E_m(t)$ is explicitly time-dependent and this time dependence maps onto the shape of the current quantization steps. To make a quantitative statement we note that the instantaneous wave-function remains unperturbed in first-order; $|\psi_N(t)|$ becomes greater than $|\psi_1(t)|$ at $t = t_0$. At this point, the partial decay widths are equal, $\Gamma_l^{(m)} = \Gamma_r^{(m)}$, and the resonance approximation yields a half-integer pumped charge. Therefore, the transition between the consecutive plateaus takes place at the gate voltages $V_g^{(m)} = E_m(t_0) - E_F$. In particular, half of the first step in the pumping curve is reached at the gate voltage

$$V_{1/2} \equiv V_g^{(1)} = V_0 + U(0, t_0), \quad (14)$$

such that $Q(V_{1/2}) = e/2$. Here $V_0 = -E_F - P - 2J_d + \Delta/2$ is the threshold voltage for the first step in the absence of perturbations.

The resonance moment associated with the left-right transition at $V_g = V_{1/2}$ is well defined, since the energy levels $E_m(t)$ are in general no longer constant in the vicinity of $t = t_0$. Therefore, the slope of the first quantization step can be estimated from the resonance approximation. The value of the total pumped charge at $V_g = V_{1/2} + \delta V$ is dominated by the unloading resonance at $t = t_0 + \delta t$, where $\delta V = \dot{E}_1(t_0)\delta t$. The other resonances contribute charges exponentially close to an integer; for simplicity, let us consider only one loading through the left lead (which gives $\Delta Q_1 \approx e = \mathrm{const.}$) before unloading at $t_0$. The contribution of the latter, $\Delta Q_2(t)$, can be calculated using the Gaussian wave-function (10) in Eqs. (7) and (8). The resulting total pumped charge $\Delta Q_1 + \Delta Q_2$ is

$$Q \approx e - \frac{e|\psi_1^{(1)}(t)|^2}{|\psi_1^{(1)}(t)|^2 + |\psi_N^{(1)}(t)|^2} = \frac{e}{2}\left(1 + \tanh\frac{Lv\delta t}{\xi^2}\right). \quad (15)$$

We define the steepness of the first step, $S$, as

$$S \equiv \left.\frac{dQ}{dV_g}\right|_{V_g = V_{1/2}} \approx \frac{eLv}{\xi^2}\left[\left|v\frac{\partial U}{\partial x} + \frac{\partial U}{\partial t}\right|^{-1}\right]_{\substack{t=t_0 \\ x=0}}. \quad (16)$$

The pre-factor in Eq. (16) is the least accurate, since the applicability of Eq. (10) at the ends of the channel is marginal. Taking the absolute value in Eq. (16) makes the result valid for both signs of $\dot{E}_1$ at $t = t_0$. Our derivation is not justified for perturbations that yield small values of the denominator in Eq. (16). Then, the steepness remains bounded due to the finite resonance width.
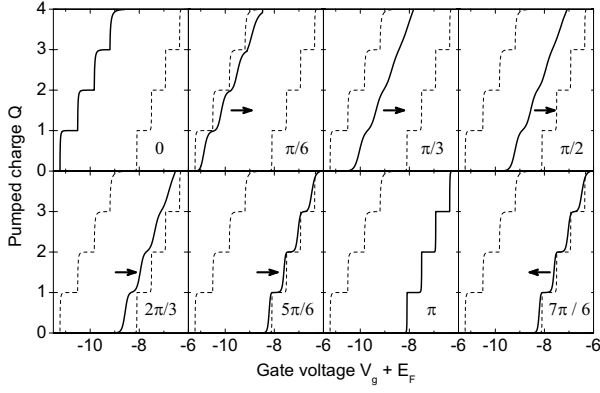
FIG. 5: Interference of two counter-propagating SAWs with an amplitude ratio $P^-/P = 0.2$. The phase difference $\varphi$ is changed from 0 to $7\pi/6$, in steps of $\pi/6$, as indicated. Solid curves show the pumped charge (in units of $e$) versus the gate voltage (in units of $J_d$), the dotted lines mark the best quantization conditions achieved at $\varphi = 0$ and $\varphi = \pi$. For $\varphi \in [\pi, 2\pi]$ the pumping curves repeat the same sequence in reverse order (not shown). The parameters used are: $P = 8J_d$, $\lambda = 4L$, $N = 10$. Curves are computed using the resonance approximation.

The quantization accuracy can be estimated along similar lines. However, the results are less transparent since the energy levels involved are beyond the simple harmonic approximation.

### A. Sensitivity to the second SAW

For a particular example of a perturbation which mimics the experimental situation, consider the following potential

$$U(x_n, t) = P^- \cos\left(\omega t + q x_n + \varphi\right) + b\, x_n/L. \quad (17)$$

Here $P^-$ and $\varphi$ are the amplitude and the phase of a second SAW, propagating in the negative direction. It can be generated either due to reflections of the main beam [2] or by a second transducer [4]. We also include a simple static perturbation [proportional to $b$ in Eq. (17)] which breaks the left-right symmetry of the channel in the absence of the SAW. The estimates in Eqs. (14) and (16) become

$$V_{1/2} = V_0 - P^- \cos\varphi, \quad (18)$$

$$S = \frac{4N_1 e}{|b + 2qLP^- \sin\varphi|}. \quad (19)$$

[We have used the relation $N_1 = L^2/(4\xi^2)$ in Eq. (19).]

First we consider the case of a reflected wave only ($b = 0$). A series of pumping curves for different values of the phase difference is presented in Fig. 5. As can be seen from Eq. (18), the threshold voltage changes periodically in $\varphi$, reaching extremal values at $\varphi = 0$ and $\pi$. Between these special values of $\varphi$, the staircase structure
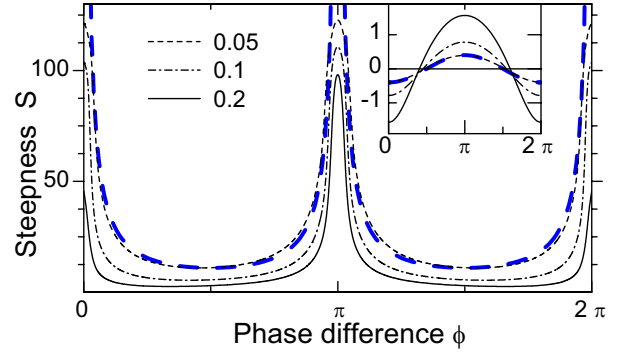


FIG. 6: (Color online) The steepness of the first step $S = dQ/dV_g$ at $Q = e(1/2)$, in units of $e\,J_d^{-1}$ for $P^-/P = 0.05, 0.1, 0.2$ as function of the phase difference $\varphi$. The curve for $P^-/P = 0.2$ corresponds to the data presented in Fig. 5. Inset: threshold voltage $V_{1/2}(\varphi) - V_0$ versus $\varphi$, in units of $J_d$. Curves are computed exactly from Eq. (4). Thick dashed (blue) lines show analytic estimates, given by Eqs. (18–19) for the smallest amplitude ratio $P^-/P = 0.05$; the pre-factor $N_1$ in Eq. (19) has been treated as a free fitting parameter. The parameters used are: $P = 8J_d$, $\lambda = 4L$, $N = 10$, $ka = \pi/5$, $\tilde{J} = 1$.

is more smooth, and the steps are more symmetric: the convex and the concave parts of a step become almost congruent. The pumping curves are identical for $\pm\varphi$ due to the symmetry of the potential (12) with $b = 0$.

For a quantitative characterization of the second SAW effect we have determined numerically the positions and the slope of the pumping curves at $Q = e/2$ without any approximations in Eq. (4). The results are shown in Fig. 6. Tuning the phase difference $\varphi$ for a fixed amplitude ratio $P^-/P$ to the values at which the r.h.s. of Eq. (19) diverges enhances the steepness of the first step by orders of magnitude. The sharpest steps are achieved at the extrema of the threshold voltage $V_{1/2}$, as shown in the inset in Fig. 6 and qualitatively in Fig. 5.

The above example shows that a symmetric pumping potential is favorable for quantization: the steepest plateaus are achieved without a secondary SAW or with $P^- \neq 0$ and $\varphi = 0, \pi$, when the total SAW potential $V(x_n, t) \equiv \epsilon_n(t)$ is invariant under $x_n \to -x_n$, $t \to -t + \text{const}$.

Further reduction of symmetry is achieved by choosing $b \neq 0$ and $P^- \neq 0$. Here two regimes are possible. For small $b$, the situation is similar to the previous case: the steepness is greatly enhanced at two values of $\varphi$ between 0 and $2\pi$, when the denominator in Eq. (19) vanishes. In contrast, for $b > 2qLP^-$ it is the static asymmetry of the channel that determines the slope of the steps, which now has only one wide maximum as function of $\varphi$. This behavior is illustrated in Fig. 7, which shows the slope of the first step as a function of the second SAW amplitude and phase. The initial steepness at $P^- = 0$, $b = 1J_d$ is $S = 12.2(e/J_d)$ for the selected model parameters. That is more than an order of magnitude less than in the unperturbed ($P^- = b = 0$) case. Increasing the
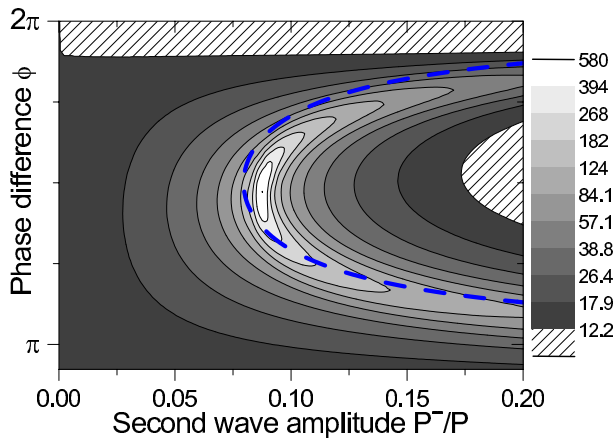
FIG. 7: (Color online) The steepness of the first step for $P = 2J_d$, $\lambda = 2L$, $N = 10$, $b = 1J_d$, as function of $P^-/P$ and $\varphi$. The dashed (blue) line marks the combinations of amplitude and phase at which the first order estimate [Eq. (19)] diverges. Note the logarithmic grey-coding scale. The steepness without the perturbation ($P^- = b = 0$) is $S = 613\,e/J_d$.

amplitude of the second SAW improves the steepness for $\pi \lesssim \varphi \lesssim 2\pi$ with a single wide maximum at $\varphi \approx 3\pi/2$, in agreement with Eq. (19). At $P^- \approx b/(2qL)$ the steepness peaks sharply, almost reaching the unperturbed value. Further increase of $P^-$ reduces the steepness gradually, which now has two maxima in $\varphi$, approaching $\varphi = \pi$ and $\varphi = 2\pi$ for large $P^-$, similarly to Fig. 6. This example shows that a weak counter-propagating SAW with properly chosen amplitude and phase is able to compensate for the static asymmetry of the pumping potential and significantly improves the sharpness of the current quantization steps.

Available experimental data are consistent with our conclusions. Periodic oscillations of $V_{1/2}$ have been observed in experiments with one active SAW transducer when the frequency of the SAW was varied. The period of these oscillations was found to match a full $2\pi$ phase shift between the main SAW and a weak wave reflected from the other (inactive) transducer [2]. Later experiments, with two active transducers on both sides of the constriction, have confirmed this scenario, and a sequence of pumping curves similar to our Fig. 5 has been reported [4]. Tuning of the second SAW amplitude and phase has enabled the authors of Ref. 4 to improve the flatness of the first quantization plateau.

The key argument leading to Eq. (19) concerns the gate voltage dependence of the potential profile at the point where capture/release of an electron happens with equal probabilities from either side of the barrier. Therefore, the phase and amplitude dependence of the steepness, $S(\varphi, P^-)$, is expected to be insensitive to the particular choice of the pumping potential, as long as it leads to a clear sequence of current quantization steps. We suggest the following generic scenario of the plateau quality improvement, that can be checked by detailed measure-

ments using existing experimental setups. One should measure the traces of the first step steepness $S(\varphi)$ as function of the reflected wave phase $\varphi$ for a set of gradually increasing secondary beam amplitudes $P^-$. At small amplitudes, $P^- < P_c^-$, the steepness is expected to have one broad maximum at some $\varphi = \varphi_0$. As $P^-$ is increased, the value at the maximum, $S(\varphi_0)$, increases and at $P^- = P_c^-$, the maximum splits into two, $S(\varphi_1)$ and $S(\varphi_2)$, with $\varphi_{1,2} = \varphi_0 \pm \arccos(P_c^-/P^-)$, as shown in Fig. 7 by the dashed line [for our model calculation $\varphi_0 = 3\pi/2$ and $P_c^- \approx b/(2qL)$].

### B. Source-drain bias and variations of screening

Experimentally, acoustoelectric current can be studied along the full crossover, from the depleted to the transmissive state of the quantum wire, by changing the voltage on the depleting gate. Our discussion so far has been concentrated on the quantized single-electron transport, which is observed in the depleted regime. As the first conduction channel opens, the shape of the pumping potential in real space as well as screening effects become increasingly important [21] and the usefulness of our simplified 1D spinless electron model is very limited. Keeping these limitations in mind, we will choose model parameters that most closely correspond to a point contact near the depletion threshold, and illustrate the breakdown of quantized transport.

For $P > J_d = \tilde{J}$, the tight-binding band is significantly deformed (see Fig. 4), therefore we choose a relatively small SAW amplitude $P = 0.5J_d$, but a large number of sites $N = 24$ to maintain $N_{\text{steps}} > 1$. The Fermi wave number $ka = \pi/12$ is taken close to the band bottom.

Consider first the situation before the SAW is applied ($P = 0$). The zero-bias dc conductance of the channel is determined by the transmission coefficient $\mathcal{T}$ (Landauer formula, see Sec. II B). There is a potential barrier between the left and the right reservoirs for $-V_g > 0$, therefore the value of $V_g + E_F = -2J_d \cos ka \approx -2J_d$ is expected to be the borderline between transmissive and blocked states of our channel. This corresponds to the depletion threshold of a true point contact. We plot the transmission coefficient in the *absence* of SAW versus gate voltage, $\mathcal{T}(V_g)$, in Fig. 8a with a thin (blue) line. For $V_g < 0$, the transmission is exponentially blocked by a rectangular barrier of height $\approx -V_g$ and length $L$, while above the depletion threshold a Fabry-Perot-like pattern of high transmission is observed due to multiple reflections at the sharp ends of the constriction.

At a non-zero SAW amplitude, the transmission coefficient $\mathcal{T}(t)$ becomes time-dependent and the adiabatic formula [Eq. (3)] should be used to relate it to the conductance. In the linear response regime, the second term in the curly brackets in Eq. (3) is proportional to $\partial^2 f/\partial E^2$ and can be neglected [22]. This results in a generalized Landauer formula [22], $G = (e^2/h)\,\mathcal{T}_{\text{av}}$, where $\mathcal{T}_{\text{av}} \equiv (\omega/2\pi)\int_0^{2\pi/\omega} dt\,\mathcal{T}(t)$ is the time average of the in-
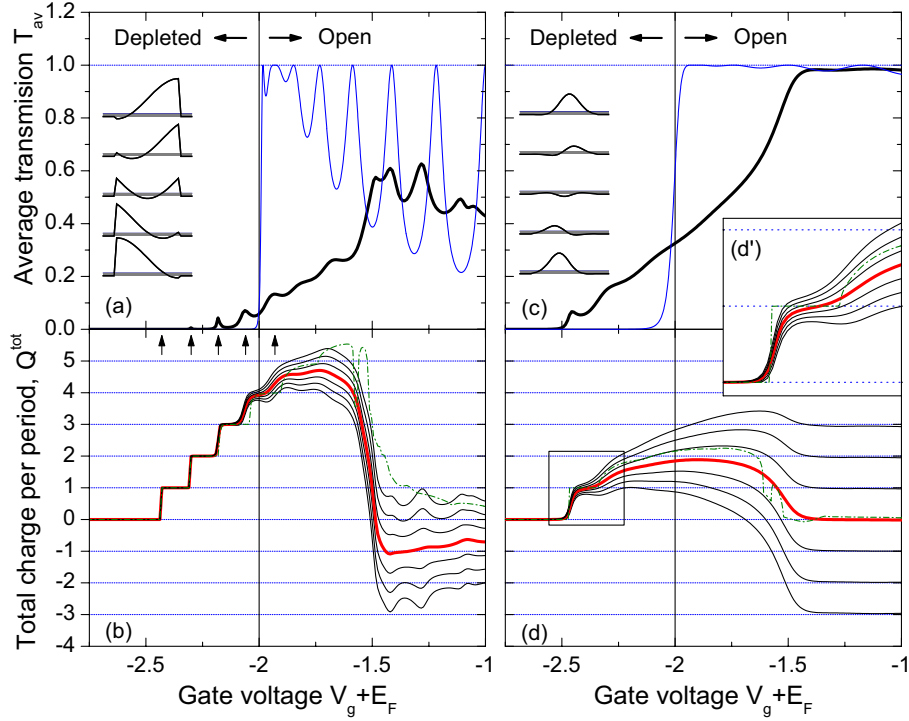
FIG. 8: (Color online) Crossover between the depleted and open regimes of the conduction channel for $N = 24$, $ka = \pi/12$, $\tilde{J} = J_d$. (a) Time-averaged transmission coefficient $\mathcal{T}_{av}$ in the absence [thin (blue) line] and presence (thick black line) of a SAW with $P = 0.5J_d$, $\lambda = 2L$. (b) The pumped charge $Q$ [thick (red) line] and the total charge $Q^{tot}$ (thin black lines) for bias voltages $eV_{SD}/(\hbar\omega)$ changing from $-3$ to $3$ in steps of one. The dashed-dotted line shows $Q^{res}$ at no bias [resonance approximation, Eq. (9)]. (c,d) The same as in (a,b), but with an exponentially screened pumping potential [Eq. (21)]. A sequence of snap-shots in panels (a,b) and (c,d) shows the corresponding pumping potential in real space for $V_g$ in the middle of the first plateau; time increases from top to bottom, $\omega t \in [\omega t_0 - \pi/2\omega; \omega t_0 + \pi/2]$.

stantaneous transmission coefficient $\mathcal{T}(t)$. This quantity is plotted in Fig. 8a with a thick black line. One can see that switching on the SAW smears the sharp step in the conductance over the range of $\pm P$ around the depletion threshold. Qualitatively similar smoothing of the conductance quantization steps due to SAW has been observed experimentally [1, 2].

Figure 8a also shows some additional structure below the depletion threshold. This structure is correlated with the pumping curve shown by a thick (red) line in Fig. 8b. Comparing $Q(V_g)$ and $\mathcal{T}_{av}(V_g)$ we see that each step in the acoustoelectric current is associated with a peak in the time averaged transmission as indicated by arrows in Fig. 8a (the first two peaks are too small to be seen on a linear scale). It is easy to explain the origin of these peaks using the resonance approximation diagram (see Fig. 2). At gate voltages between the quantization plateaus the system remains at resonant transmission for a considerable fraction of the period, therefore $\mathcal{T}_{av}$ becomes greatly enhanced.

In the presence of both SAW and source-drain bias, the total charge transfer per period, $Q^{tot} \equiv \int_0^{2\pi/\omega} dt\, I_l(t)$, becomes

$$Q^{tot} = Q + (e^2 V_{SD}/\hbar\omega)\, \mathcal{T}_{av} \qquad (20)$$

(in the linear response regime). The result is a sum of the two terms: pure pumping contribution [thick (red) curve in Fig. 8b]; and the average transmission (thick curve in Fig. 8a), multiplied by a constant. Equation (20) suggests that $\hbar\omega$ is a natural unit for the source-drain energy mismatch $eV_{SD}$. In the quantized pumping region, the contribution of the bias, $I^{bias}$, becomes comparable to that of pumping, $I^{pump}$, if the bias voltage source transports several electrons per cycle. When $\mathcal{T}_{av}$ is of order one, this regime is attained for $eV$ equal to several $\hbar\omega$. Thus for a qualitative picture of the pumping curve in the presence of bias, we have plotted $Q^{tot}$ for the bias voltage $eV_{SD}/\hbar\omega$ ranging from $-3$ to $3$ by thin black lines in Fig. 8b. The main observation is that the higher is the step number the more sensitive it is to the bias (as one can already appreciate form the average transmission curve). Similar behavior is reported in experimental studies [1, 2].

The main results of the above discussion remain unchanged if a phenomenological screening [13, 21] is introduced:

$$\epsilon_n(t) = [-V_g + P \cos(\omega t - q x_n)] \exp\left(-x_n^2/L_s^2\right). \qquad (21)$$

We have repeated the previous calculation using the same values of parameters but modified the pumping potential

(21) with $L_s = L/4 = \lambda/8$. The results are shown in Figs. 8c and 8d. The main qualitative difference is the disappearance of the interference pattern in the transmission curve both with and without the SAW. The number of steps is reduced to one (shown separately in Fig. 8d′), since the effective amplitude of the SAW is decreased by the screening factor in Eq. (21). Calculations with larger values of $P$ produce more steps, along the same lines as discussed in Sec. III B for the unscreened potential (1). We have also checked that the behavior of the first step steepness $S(P^-, \varphi)$ as function of reflected SAW amplitude and phase, follows the general scenario suggested in Sec. IV A.

We note that in the above example (Fig. 8) the resonance approximation still holds below the depletion threshold, when a moving quantum well is isolated from the Fermi sea in the leads.

## V. DISCUSSION AND CONCLUSIONS

Quantized electronic transport, driven by SAW's, has been considered in several recent theoretical studies [10, 11, 12, 13, 14, 15, 17]. Here we discuss our approach in relation to those works.

Several of models [10, 11, 12, 15] make a distinction between electrons *already localized* in a moving potential well (dynamic quantum dot) and those belonging to the Fermi sea. The current is then calculated by considering the loss of electrons from the dynamic quantum dot at the stage of its formation [12, 15] and/or its subsequent motion [10, 11, 12, 15]. This approach presupposes the formation of the dynamic quantum dot, but does not require it to be at thermodynamic equilibrium with the reservoirs at all times. Moreover, all the quantization error mechanisms within these models (gradual back-tunneling [10, 11, 12], non-adiabaticity at the formation stage [12] and non-equilibrium dynamics during the transfer [15]) consider electrons with energies that can significantly exceed the Fermi energy in the remote reservoirs.

Our adiabatic quantum calculation [16] differs from these studies in two significant aspects: (i) The formation of a dynamic quantum dot is not a necessary condition for the calculation of the acoustoelectric current. We do identify, however, the localized electronic states (whenever such states are present) via the resonance approximation and confirm that they are responsible for the quantized transport. (ii) In the adiabatic pumping approximation [22], the time-dependent potential never excites the carrier by a finite amount of energy away from the Fermi level [29]. Therefore, we never observe quantization steps when the moving potential well rises above the Fermi level upon passing through the middle of the channel.

We find the numerical calculations by Maksym [13] to be the closest to our study. He considers a 1D single-particle model with a pumping potential similar to our Eq. (21). The current at the quantization plateaus is found to be carried by the lowest energy states of the local potential minimum, in accordance with our results.

The quantization accuracy in our approach is determined by two factors which we expect to become experimentally relevant for sufficiently low tunnelling barriers. The first one is the possibility of *both* reservoirs to participate in the capture/release of an electron. This error mechanism is covered by the resonance approximation and leads to simple estimates like our formulas for the first step steepness discussed in Sec. IV A. The second factor concerns mixing of the localized states with continuum in the leads, which can give significant width to the quasi-stationary states in the moving quantum dot. Compared to the predictions of the loading/unloading scenario (Sec. II C), this effect further degrades the flatness of the quantization (see, e.g., Figs. 3b, 6 and 8d) and eventually leads to the breakdown of the quantized transport as the channel opens (Sec. IV B).

We have not considered explicit Coulomb interactions between electrons in the depleted part of the channel, which set the energy scale of the problem. One can make a naive estimate of the level spacing $\Delta$, which in the continuous limit is [16] $\Delta = \hbar q \sqrt{P/m^*}$. Using typical experimental values [4] for the SAW amplitude $P = 20$meV, wavelength $\lambda = 1\mu$m and GaAs bulk effective mass $m^\star = 0.067m_0$, one gets $\Delta = 1$meV, which is an order of magnitude less that the distance between the quantization steps observed in experiments [1, 2, 4]. This discrepancy can be qualitatively understood on a mean-field level: if an electron is captured by the moving potential minimum, its unscreened electric field makes the potential well seen by the other electrons much shallower, and thus increases the spacing $\Delta$ between resonances by the amount of the charging energy [30, 31]. Such a picture is also supported by the numerical calculation of a two-electron problem by Gumbs and co-workers [11]. It is plausible that the effective values for the parameters of our model can be estimated from a self-consistent realistic calculation.

In conclusion, we have considered a simple model for SAW-driven adiabatic pumping of electrons through a quasi-1D quantum wire. A stair-case structure of the acoustoelectric current has been mapped onto the instantaneous energy spectrum of the pumping potential. Numerical calculations and analytic estimates confirm the experimentally observed behavior of the acoustoelectric current as function of the SAW amplitude, wavelength, source-drain bias, and the parameters of a weak counter-propagating beam. Quantitative measurements of the plateau quality as a function of the second SAW amplitude and phase are proposed to probe the relevance of our model. The presented single-electron picture captures all the main features of the quantized transport.

11

[1] J. M. Shilton, V. I. Talyanskii, M. Pepper, D. A. Ritchie, J. E. F. Frost, C. J. B. Ford, C. G. Smith, and G. A. C. Jones, J. Phys. C **8**, L531 (1996).

[2] V. I. Talyanskii, J. M. Shilton, M. Pepper, C. G. Smith, C. J. B. Ford, E. H. Linfield, D. A. Ritchie, and G. A. C. Jones, Phys. Rev. B **56**, 15 180 (1997).

[3] V. I. Talyanskii, J. M. Shilton, J. Cunningham, M. Pepper, C. J. B. Ford, C. G. Smith, E. H. Linfield, D. A. Ritchie, and G. A. C. Jones, Physica B **249–251**, 140 (1998).

[4] J. Cunningham, V. I. Talyanskii, J. M. Shilton, M. Pepper, M. Y. Simmons, and D. A. Ritchie, Phys. Rev. B **60**, 4850 (1999).

[5] J. Cunningham, V. I. Talyanskii, J. M. Shilton, M. Pepper, A. Kristensen, and P. E. Lindelof, Phys. Rev. B **62**, 1564 (2000).

[6] J. Ebbecke, G. Bastian, M. Blöcker, K. Pierz, and F. J. Ahlers, Appl. Phys. Lett. **77**, 2601 (2000).

[7] J.-T. Janssen and A. Hartland, IEEE Transactions on instrumentation and measurement **50**, 227 (2001).

[8] A. M. Robinson, V. I. Talyanskii, M. Pepper, J. E. Cunningham, E. H. Linfield, and D. A. Ritchie, Phys. Rev. B **65**, 045313 (2002).

[9] N. E. Fletcher, J. Ebbecke, T. J. B. M. Janssen, F. J. Ahlers, M. Pepper, H. E. Beere, and D. A. Ritchie, Phys. Rev. B **68** (2003), cond-mat/0308402.

[10] G. R. Aĭzin, G. Gumbs, and M. Pepper, Phys. Rev. B **58**, 10 589 (1998).

[11] G. Gumbs, G. R. Aĭzin, and M. Pepper, Phys. Rev. B **60**, 13 954 (1999).

[12] K. Flensberg, Q. Niu, and M. Pustilnik, Phys. Rev. B **60**, 16 291 (1999).

[13] P. A. Maksym, Phys. Rev. B **61**, 4727 (2000).

[14] Y. M. Galperin, O. Entin-Wohlman, and Y. Levinson, Phys. Rev. B **63**, 153309 (2001).

[15] A. M. Robinson and C. H. W. Barnes, Phys. Rev. B **63**, 165418 (2001).

[16] A. Aharony and O. Entin-Wohlman, Phys. Rev. B **65**, 241401 (2002), cond-mat/0111053.

[17] V. A. Margulis, M. P. Trushin, and A. V. Shorokhov, JETP **94**, 1160 (2002).

[18] O. Entin-Wohlman, A. Aharony, and V. Kashcheyevs, J. Phys. Soc. Japan **72A**, 77 (2003), cond-mat/0201073.

[19] J. L. Flowers and B. W. Petley, Rep. Prog. Phys. **64**, 1191 (2001).

[20] C. H. W. Barnes, J. M. Shilton, and A. M. Robinson, Phys. Rev. B **62**, 8410 (2000).

[21] Y. Levinson, O. Entin-Wohlman, and P. Wölfle, Phys. Rev. Lett. **85**, 634 (2000).

[22] O. Entin-Wohlman, A. Aharony, and Y. Levinson, Phys. Rev. B **65**, 195411 (2002), cond-mat/0201073.

[23] V. Kashcheyevs, A. Aharony, and O. Entin-Wohlman (2003), submitted to PRB, cond-mat/0308382.

[24] M. Büttiker, H. Thomas, and A. Prêtre, Z. Phys. B **94**, 133 (1994).

[25] P. W. Brouwer, Phys. Rev. B **58**, 10 135 (1998).

[26] R. Landauer, Philosophical Magazine **21**, 863 (1970).

[27] O. Entin-Wohlman and A. Aharony, Phys. Rev. B **66**, 035329 (2002).

[28] Y. Levinson, O. Entin-Wohlman, and P. Wölfle, Physica A **302**, 335 (2001), cond-mat/0010494.

[29] M. Moskalets and M. Büttiker, Phys. Rev. B **66**, 205320 (2002), cond-mat/0208356.

[30] M. V. Moskalets, Phys. Rev. B **63**, 113309 (2001).

[31] R. Berkovits, F. von Oppen, and J. W. Kantelhardt (2003), unpublished, cond-mat/0307730.